

The Chemical composition of the post-AGB F-supergiant CRL 2688

Miho N. Ishigaki¹ \star , Mudumba Parthasarathy^{1,2}, Bacham E. Reddy³,
Pedro García-Lario⁴, Yoichi Takeda¹, Wako Aoki¹,
D. A. García-Hernández^{5,6}, and Arturo Manchado^{5,6}

¹*National Astronomical Observatory of Japan, 2-21-1 Osawa, Mitaka, Tokyo 181-8588, Japan*

²*Aryabhata Research Institute of Observational Sciences, Nainital, India*

³*Indian Institute of Astrophysics, Bangalore 560034, India*

⁴*Herschel Science Centre, European Space Astronomy Centre, Villafranca del Castillo, P.O. Box 78, E-28080 Madrid, Spain*

⁵*Instituto de Astrofísica de Canarias, 38200, La Laguna, Tenerife, Spain*

⁶*Departamento de Astrofísica, Universidad de La Laguna, 38200, La Laguna, Tenerife, Spain*

ABSTRACT

We present an analysis of a high resolution ($R \sim 50,000$) optical spectrum of the central region of the proto-planetary nebula CRL 2688. This object is thought to have recently moved off the AGB, and display abundance patterns of CNO and heavy elements that can provide us with important clues to understand the nucleosynthesis, dredge-up and mixing experienced by the envelope of the central star during its AGB stage of evolution. The analysis of the molecular features, presumably originated from the circumstellar matter provides further constraints on the chemistry and velocity of the expanding shell, expelled as a consequence of the strong mass loss experienced by the central star.

We confirm that the central star shows a spectrum typical of an F-type supergiant with $T_{\text{eff}} = 7250 \pm 400$ K, $\log g = 0.5$ and $[\text{Fe}/\text{H}] = -0.3 \pm 0.1$ dex. We find that the abundance pattern of this object is characterized by enhancements of Carbon ($[\text{C}/\text{Fe}] = 0.6 \pm 0.1$), Nitrogen ($[\text{N}/\text{Fe}] = 1.0 \pm 0.3$) and Na ($[\text{Na}/\text{Fe}] = 0.7 \pm 0.1$), similar to other previously known carbon-rich post-AGB stars. Yttrium is also enhanced while the $[\text{Ba}/\text{Y}]$ ratio is very low (-1.0), indicating that only the light s-process elements are enhanced. The Zinc abundance is found to be normal, $[\text{Zn}/\text{Fe}] = 0.0 \pm 0.3$, suggesting that there is no depletion of refractory elements. The $\text{H}\alpha$, Na I and K I resonance lines show prominent emission components, whose helio-centric radial velocities are offsetted by -41 ± 3 km s⁻¹ relative to the photospheric metal-absorption lines. The molecular features of C₂ and CN also show emission components, whose velocities are consistent with the emission components of the $\text{H}\alpha$, Na I and K I lines. On the other hand, their absorption components are more highly blue shifted than the corresponding emission components, which suggests that the regions where the emission and absorption components arise are expanding at different velocities.

Key words: stars: AGB and post-AGB - stars: evolution -stars: abundances- stars: circumstellar matter -stars: individual (CRL2688).

1 INTRODUCTION

CRL 2688 (V1610 Cyg, Egg Nebula) is a bipolar proto-planetary nebula (PPN). The central star is thought to be a F5Iae post-AGB supergiant. Initial studies of CRL 2688 were mostly based on low res-

olution spectrophotometric and spectropolarimetric data and were made by Ney et al. (1975), Forrest et al. (1975), Crampton, Cowley & Humphreys (1975) and Cohen & Kuhi (1977, 1980). The low resolution spectrophotometric observations revealed emission from C₂, C₃ and SiC₂. The Swan bands of C₂ are also seen in emission from the bipolar lobes (Cohen & Kuhi 1980). Because the object is faint ($V = 13.5$) with significant

\star E-mail:ishigaki.miho@nao.ac.jp

circumstellar reddening its high resolution spectroscopy was not carried out until the year 2000. The first high resolution ($R = 15,000$) optical spectra were analyzed by Klochkova et al. (2000). They found that the central star is a F5Iae post-AGB supergiant with overabundance of carbon and s-process elements. Klochkova et al. (2000) derived $T_{\text{eff}} = 6500$ K, $\log g = 0.0$, microturbulent velocity $= 6.0$ km s $^{-1}$ and $[\text{Fe}/\text{H}] = -0.59$.

High-spatial resolution *Hubble Space Telescope* imaging revealed the detailed morphology of this object; a flattened dust cocoon obscuring the central star as well as extended bipolar nebulae exhibiting numerous concentric arcs crossed by a pair of beam-like structures at the both sides of the equatorial plane (Sahai et al. 1998). These arcs are suggested to be associated with repeated mass-loss events during the AGB phase (Sahai et al. 1998; Balick et al. 2012).

Recently, Wesson et al. (2010) studied the *Herschel Space Observatory* - SPIRE FTS spectra of CRL 2688 covering the wavelength range 195 to 670 μm . They found the far infrared spectrum of CRL 2688 to be very complex with about 18 different species of complex molecules. They also detected water in CRL 2688 for the first time.

CRL 2688 shows small amplitude light variations with a period of about 90 days (Hrivnak et al. 2010) and some of the absorption and emission lines seems to show a radial velocity variability with time (Klochkova et al. 2000). The variability indicates that the central star as well as the circumstellar material is undergoing rapid variations in their dynamical and chemical properties possibly due to pulsation and mass-loss.

Mechanisms that give rise to observed complex morphology, chemistry and variability of CRL 2688 as well as other post-AGB stars are still far from being completely understood. Identifying constraints on these mechanisms is important for understanding the chemical evolution of our Galaxy since low-to-intermediate mass stars on the AGB phase of evolution are thought to be mainly responsible for synthesizing and contributing with CNO and s-process elements to the interstellar medium via mass loss.

In this paper we present an analysis of a much higher resolution spectrum of CRL 2688.

2 OBSERVATION AND REDUCTION

A high resolution ($R \sim 50,000$) spectrum of CRL 2688 was obtained with the Utrecht Echelle Spectrograph (UES) at the 4.2 m William Herschel Telescope on July 14, 2001. The slit of 1 arcsec widths was positioned at the central star region. The wavelength range from 4300 to 9000 \AA was observed with an exposure time of 1200 sec. The data were reduced with standard IRAF routines. The signal to noise ratio of the reduced spectrum per resolution element varies from 30 to 70 in this wavelength range.

Equivalent widths (EW) of atomic absorption lines were measured by fitting Gaussian to each feature using a linelist described below.

3 DESCRIPTION OF THE SPECTRUM

The reduced spectrum shows various photospheric absorption lines and molecular lines. A portion of the observed spectrum is shown in Figure 1. Absorption lines that are considered in the EW measurements taken from Reyniers et al. (2004) and Klochkova et al. (2000) are marked.

3.1 Atomic lines

The obtained optical spectrum of CRL 2688 exhibits numerous atomic absorption lines of metals, most of which are too weak to be used in the abundance analysis, as illustrated in Figure 1. Many of the relatively strong lines like $\text{H}\alpha$ and Ba II show a blueshifted emission component superimposed on the absorption component as shown in Figure 2. The presence of emission component in the $\text{H}\alpha$ violet wing is in agreement with the suggestion from a spectropolarimetric observation of Klochkova et al. (2004). The observed features indicate mass loss from the central star.

3.2 Molecular lines

The molecular lines in this star are likely originated from its circumstellar envelope, because such molecules would be destroyed in its photosphere with $T_{\text{eff}} \sim 7000$ K. The spectral regions dominated by molecular bands are shown in Figure 3 and 4.

Strong emission bands of the C_2 Swan system are identified consistent with previous studies (Crampton, Cowley & Humphreys 1975; Cohen & Kuhi 1980; Klochkova et al. 2000, 2004). The particularly strong band at 5635.5 \AA of $\text{C}_2(0,1)$ is shown in the middle panel of Figure 3. Cohen & Kuhi (1977) showed that the C_2 emission bands are prominently seen only in unpolarized light. The negligible polarization for the C_2 Swan emission bands has also reported by the study of Klochkova et al. (2004) with a much higher-resolution spectropolarimetry, suggesting that the observed C_2 emission may come directly from the line forming region.

We confirm the presence of molecular absorption bands of the C_2 Phillips system and the CN red system, as shown in Figure 4. The detection of these molecular absorption bands had previously been reported by Bakker et al. (1997). Additionally, some of the features in C_2 Phillips (2,0) and (3,0) bands are shown in emission, whose central wavelength is less blue shifted than the corresponding absorption component. A few transitions in the CN (2,0) band also appear to show emission components.

Cohen & Kuhi (1980) have suggested the presence of the Merrill-Sanford bands of SiC_2 in absorption, strongest at 4977 \AA , particularly in the region of the nebular lobe. Our spectrum does not show this feature in agreement with the apparent lack of this feature in the study of the central region of CRL 2688 made by Cohen & Kuhi (1980).

3.3 Na I and K I resonance lines

Figure 5 shows portions of the spectrum around Na I and K I resonance lines. Na I lines are expected to have contribution from stellar photosphere, circumstellar envelope and interstellar matter. However as we will indicate in Section 3.4,

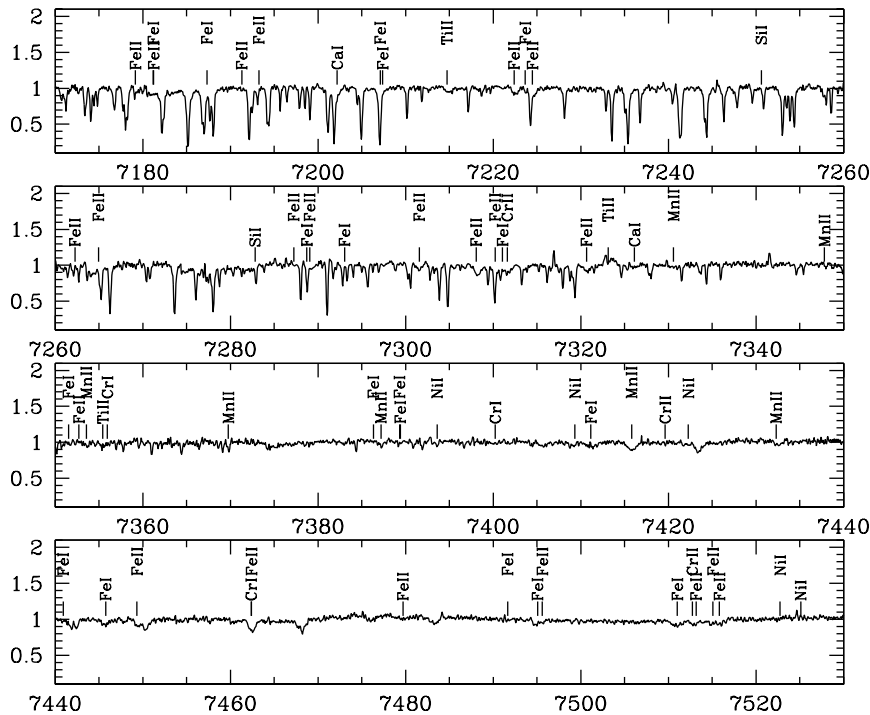


Figure 1. A portion of the obtained spectrum of CRL2688. Positions of metal-lines used in the EW determination are indicated.

[htbp]

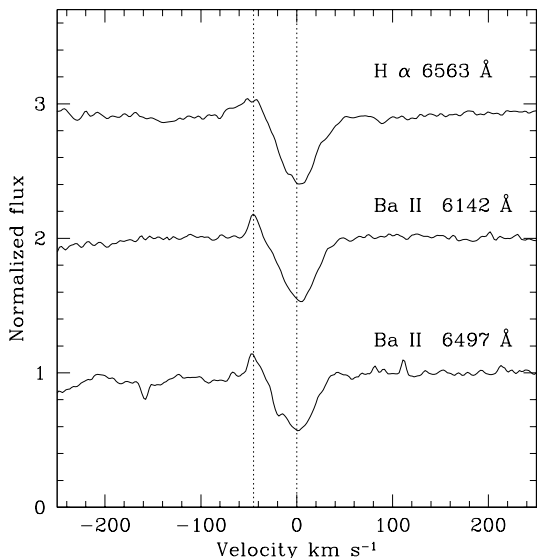


Figure 2. Line profile for H α and Ba II lines. Only the core region of the line profile is shown for the H α line. All lines are shifted in velocity relative to the photospheric one.

contribution from the interstellar absorption is likely small for this object. The observed Na I D1 and D2 lines show a complex structure showing multiple components. Each of the D1 and D2 line shows at least two emission components ('e1' and 'e2' in the top panel of Figure 5). The stronger

component ('e1') is blueshifted while the weaker component ('e2') is located close to the restframe wavelength. The K I lines of this star are likely of circumstellar origin since K would be mostly ionized in the photosphere. Similar to the Na I lines, the K I line shows both absorption and emission components ('a1', 'a2' and 'e1'). The absorption component, which is at the bluer side of the emission feature, appear to show at least two velocity components.

Signatures of multiple components of Na I and K I absorption features have been reported in other post-AGB stars, like e.g. in HD 56126 (Bakker et al. 1996; Crawford & Barlow 2000). Based on a very high-resolution ($R \sim 900000$) observations of this object, Crawford & Barlow (2000) reported that the K I absorption feature of this object shows multiple components, some of which have a counterpart in C₂ molecular features. They suggested that the individual components are associated with distinct shells of circumstellar matter around this object. Higher resolution spectroscopy is clearly needed to address the nature of the shape of Na I and K I lines in CRL 2688 by resolving their intrinsic profiles.

Klochkova et al. (2004) reported that the Na I emission component is likely unpolarized, suggesting that it is came directory from the observed lobe region. The presence of the emission components in both Na I and K I lines as seen in CRL 2688 has also been observed in a number of other C-rich (and O-rich) post-AGB stars (Luna et al. 2008), although some of the similar class of objects like IRAS 06530-0123 do not seem to show these emissions (Hrivnak & Reddy 2003).

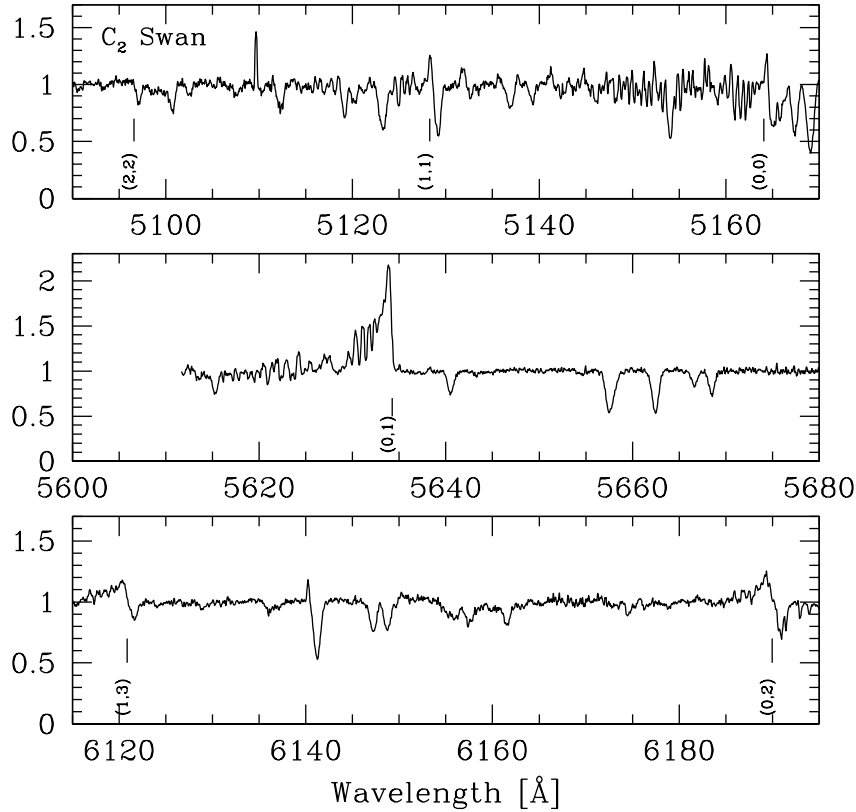


Figure 3. The observed spectrum of the C_2 Swan system. The C_2 emission features are indicated based on the identification by Cohen & Kuhi (1977).

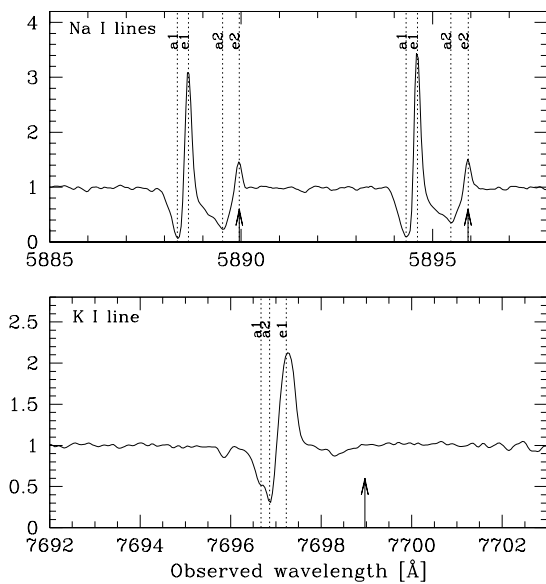


Figure 5. Na I and K I lines. Emission and absorption components for which radial velocities of the line center have been measured are indicated by dotted lines. Their restframe wavelengths are indicated by arrows.

3.4 Diffuse interstellar bands

Equivalent widths of diffuse interstellar bands (DIBs) have been calibrated to estimate the line-of-sight reddening ($E(B-V)$) (Friedman et al. 2011). In the present spectrum of CRL2688, most of the reported strong DIBs are too weak or likely contaminated by neighboring spectral features. The well calibrated DIB centered at 5780.5 Å may also be contaminated by photospheric absorption lines. Even though, it may be useful to estimate an upper limit of $E(B-V)$ toward the line-of-sight of CRL 2688. Note that a Doppler shift of the observed DIB is not consistent with that of the molecular absorption and emission lines, which indicates the DIB is originated from interstellar matter rather than from circumstellar envelope. Indeed, Luna et al. (2008) did not detect signatures of the diffuse bands of circumstellar origin for a representative sample of Galactic post-AGB stars.

The equivalent width of the feature near 5780.5 Å is 67 mÅ. According to the calibration of Friedman et al. (2011), this corresponds to $E(B-V) = 0.1$, suggesting that the interstellar reddening is very low at the line-of-sight of this object. Although CRL 2688 is located at low Galactic latitude at $(l, b) = (80.166, -6.502)$, where integrated reddening is $E(B-V) = 0.28$ according to Schlegel et al. (1998), the low $E(B-V)$ value may be reasonable since the distance to this object was estimated to be only 420 pc (Ueta et al. 2006). On the other hand, photometric observation of Ney et al.

(1975) suggests that the extinction toward this object in visual wavelengths is at least 3 mag. If the interstellar reddening is very low as suggested by the present analysis, most of the extinction toward the CRL 2688 is due to the circumstellar matter and the dusty disk.

4 RADIAL VELOCITY

Radial velocities from unblended metal absorption lines have been measured by fitting Gaussian to individual features. For the spectral lines containing both emission and absorption components, we have only used a core region of each feature to determine its central wavelength with the IRAF *splot* routine. In the following, all radial velocities are those corrected to helio-centric values (V_{\odot}). Table 1 summarizes heliocentric radial velocities obtained from the observed spectral features.

The mean of radial velocities from unblended metal absorption lines is -14.4 ± 0.6 km s $^{-1}$, which represents the radial velocity of the central star. The standard deviation of the radial velocities from individual lines is $\sigma = 2.7$ km s $^{-1}$. In the following, an error in a velocity measured from a single line is taken to be equal to this value. The V_{\odot} measured from our spectrum is in good agreement with that obtained by Klochkova et al. (2000, 2004) using metal-lines in the spectrum, although the observed spectrum by Klochkova et al. (2000, 2004) is that of the northern lobe of CRL 2688, while the present study is based on the spectrum of the central star.

Emission components of H α , Na I ('e1' in Figure 5) and K I lines all show similar radial velocity with a mean -55 km s $^{-1}$ with respect to their rest frame wavelength. This value is smaller in magnitude by more than ~ 20 km s $^{-1}$ from that obtained from the emission component of H α by Klochkova et al. (2000). As reported by Klochkova et al. (2000), the emission components also displayed some variability in time. Therefore, the observed difference in the radial velocity may be attributed to both spatial and time variations possibly due to the circumstellar outflow. The weaker emission components in the Na I D1 and D2 lines ('e2' in Figure 5) marginally agree with lab wavelengths. Therefore, it is likely that the e2 components in the Na I D1 and D2 lines are due to night sky emission and/or there may be some contribution from CRL 2688.

The absorption component in the H α line shows the radial velocity of -10.6 ± 2.7 km s $^{-1}$. This value is 3.8 km s $^{-1}$ smaller in magnitude than that from metal lines. This difference could be attributed to the presence of emission line in its violet wing, modifying the true central wavelength of the absorption feature. Similarly, Na I D1 and D2 lines show a broad absorption feature ('a2' in Figure 5) with a violet wing. The radial velocity of this feature is -10.6 and -10.0 km s $^{-1}$ for the D1 and D2 lines, which are similar to the absorption component of H α . Another absorption components ('a1' in Figure 5) of the Na I lines have radial velocity of -69.8 km s $^{-1}$. This value is close to the absorption component ('a2' in Figure 5) of the K I line.

The emission components of individual features in C₂ Phillips (3,0) and (2,0) bands show radial velocity of -53.3 ± 0.9 and -51.7 ± 1.0 km s $^{-1}$, respectively, that are marginally consistent with those of the H α , Na I and K I lines. For the

Table 1. Radial velocities

Features	V_{\odot} (km s $^{-1}$)	
	absorption	emission
Metal lines	-14.4 ± 0.6	—
H α^a	-10.6	-55.0
Na I D1	$-69.7, -10.6$	$-54.8, 12.7$
Na I D2	$-69.9, -10.0$	$-55.1, 12.3$
K I	$-77.15, -69.67^b$	-55.2
C ₂ Phillips (3,0)	$-67.2 \pm 0.2(3)^c$	$-53.3 \pm 0.9(5)$
C ₂ Phillips (2,0)	$-67.5 \pm 0.6(3)$	$-51.7 \pm 1.0(5)$
CN red (3,0)	$-65.5 \pm 0.2(3)$	—
CN red (2,0)	$-66.8 \pm 0.5(4)$	—

^a Errors in V_{\odot} measured from a single line are assumed to be 2.7 km s $^{-1}$, which is equal to the scatter (σ) in V_{\odot} from the metal lines.

^b Deblending and fitting were not successfully made. The values for approximate local minima are given.

^c Number of lines used to measure the mean V_{\odot} for each band.

CN red system, the radial velocities for the different emission components are difficult to measure because the emission features are weak and appeared to be affected by blending.

On the other hand, the absorption components of the C₂ Phillips bands have a mean radial velocity of -67 km s $^{-1}$, which is more highly blue shifted than the corresponding emission components, while the absorption components of the CN red system show a similar radial velocity of -66 km s $^{-1}$.

5 ABUNDANCE ANALYSIS

The abundance analysis is performed using a LTE abundance analysis code as in Aoki et al. (2009) together with Kurucz NEWODF model atmosphere (Castelli & Kurucz 2003) using the EWs measured for the atomic absorption lines. In order to exclude the features with erroneous fitting, we restrict the lines used in the abundance analysis to those with a FWHM in a range 0.4 to 1.0, where typical FWHM of the metal absorption lines in our spectrum is 0.7 Å. We also exclude very strong lines with $\log(EW/\lambda) \geq -4.4$. The measured EWs with these criteria are used in the abundance analysis and are listed in Table 2.

5.1 Atomic data

We have adopted a linelist compiled from Klochkova et al. (2000) and Reyniers et al. (2004). The adopted $\log gf$ values and measured equivalent widths are summarized in Table 2.

5.2 Atmospheric parameters

The effective temperature (T_{eff}) of CRL 2688 was derived using the Fe I excitation equilibrium, in such a way that the trend of the Fe abundances from individual Fe I lines with their excitation potentials is minimized within 0.04 dex eV $^{-1}$, which is the typical error of the slope. This yields

Table 2. Equivalent widths

Elem	λ (Å)	$\log gf$ (dex)	χ (eV)	EW (mÅ)	Ref. ^a
C I	4775.90	-2.19	7.49	136.29	R04
C I	5039.06	-1.77	7.95	98.71	R04
C I	6013.16	-1.16	8.65	94.61	R04
C I	6014.83	-1.58	8.64	63.62	R04
C I	7113.18	-0.93	8.65	100.95	K00
N I	7468.31	-0.17	10.34	147.93	R04
O I	6158.19	-0.31	10.74	119.67	R04
Na I	5682.63	-0.67	2.10	43.70	R04
Na I	5688.21	-0.37	2.10	117.00	R04
Si II	5056.02	0.31	10.03	172.29	R04
Si II	5978.93	-0.06	10.07	81.26	K00
S I	6041.92	-1.00	7.87	21.87	K00
S I	6743.58	-0.56	7.87	36.05	R04
S I	6757.16	-0.20	7.87	65.03	R04
Ca I	5857.46	0.24	2.93	72.66	K00
Ca I	6439.07	0.39	2.53	111.29	R04
Ca I	6462.57	0.31	2.52	102.07	R04
Ca I	6717.69	-0.52	2.71	50.41	K00
Sc II	5640.99	-1.01	1.50	194.12	K00
Sc II	5667.15	-1.21	1.50	112.34	R04
Sc II	5669.04	-1.09	1.50	186.12	K00
Sc II	5684.20	-1.01	1.51	188.86	K00
Ti II	4798.52	-2.67	1.08	158.12	R04
Ti II	5418.80	-2.17	1.58	178.38	K00
Cr II	4812.35	-1.80	3.86	153.08	R04
Cr II	5246.77	-2.47	3.71	107.48	R04
Cr II	5249.43	-2.62	3.76	86.20	K00
Cr II	5305.87	-2.08	3.83	136.25	R04
Cr II	5308.43	-1.81	4.07	112.35	R04
Cr II	5334.87	-1.89	4.07	196.78	R04
Cr II	5407.60	-2.15	3.83	102.92	R04
Cr II	5420.92	-2.46	3.76	110.42	R04
Mn I	4783.42	0.04	2.30	66.73	R04
Fe I	4966.09	-0.84	3.33	62.76	R04
Fe I	5049.82	-1.35	2.28	50.84	R04
Fe I	5302.30	-0.88	3.28	79.74	K00
Fe I	5364.87	0.23	4.45	67.96	R04
Fe I	5367.47	0.44	4.42	84.23	R04
Fe I	5393.17	-0.91	3.24	86.78	K00
Fe I	5405.77	-1.84	0.99	163.20	K00
Fe I	5434.52	-2.12	1.01	97.56	R04
Fe I	5445.04	0.04	4.39	55.27	R04
Fe I	5446.92	-1.93	0.99	162.08	K00
Fe I	6024.06	-0.06	4.55	71.55	R04
Fe I	6230.72	-1.28	2.56	28.13	R04
Fe I	6400.00	-0.29	3.60	59.87	R04
Fe II	5991.37	-3.56	3.15	151.98	R04
Fe II	6084.10	-3.80	3.20	108.07	R04
Fe II	6416.92	-2.85	3.89	195.32	K00
Fe II	6432.68	-3.71	2.89	144.65	R04
Fe II	7711.71	-2.74	3.90	181.66	K00
Ni I	5035.37	0.29	3.63	87.94	R04
Zn I	4810.54	-0.17	4.08	28.38	R04
Y II	5289.81	-1.85	1.03	46.98	R04
Y II	5728.89	-1.12	1.84	168.35	K00
Ba II	5853.67	-1.00	0.60	228.35	K00

^a Reference for $\log gf$. R04: Reyniers et al. (2004), K00: Klochkova et al. (2000)

$T_{\text{eff}} = 7250 \pm 400$ K. This value is higher than the previous estimate by Klochkova et al. (2000), ($T_{\text{eff}} = 6500$ K with a typical uncertainty of 200 K) but in good agreement with that obtained by Bakker et al. (1997) ($T_{\text{eff}} = 6900$ K) within the quoted error. The surface gravity ($\log g$) is estimated from the Fe I and Fe II ionization balance. The model atmosphere with $\log g = 0.5$ dex, which is a lower limit of $\log g$ in the available model grids with $T_{\text{eff}} > 7000$ K, yields reasonable agreement between the Fe abundances based on the neutral and ionized species. Finally, the micro-turbulence velocity ξ is estimated by minimizing the Fe I abundance

versus equivalent widths correlation. This results in $\xi = 6.5$ km s⁻¹ which agrees with that from Klochkova et al. (2000).

5.3 Abundances

Adopting the atmospheric parameters estimated above, we have obtained abundances of C, N, O, Na, α elements, Fe-peak elements and neutron capture elements from the measured equivalent widths. For heavy neutron-capture elements, spectral synthesis have been applied, which gives upper limits in the abundances. In the following, we have taken an error as a line-to-line scatter divided by the square root of the number of lines (e.g. an error in the mean of the abundances from individual lines). When only one line is available for the abundance estimate, then an error is taken to be equal to 0.25, which is the line-to-line scatter in abundances derived from individual Fe I lines.

However, uncertainty from systematic errors may be much larger than the random errors from the line-to-line scatter. Systematic errors due to the adopted atmospheric parameters are checked by changing the parameters by $\Delta T_{\text{eff}} = \pm 400$ K, $\Delta \log g = +0.5$ dex (a model atmosphere with $\log g = 0.0$ dex is not available) and $\Delta \xi = \pm 2.0$ km s⁻¹. The results of this exercise and obtained [X/Fe] values are summarized in Table 3. Typically, changes in [X/Fe] values are < 0.3 dex for the change in the T_{eff} and < 0.1 dex for the change in the $\log g$, except for [N/Fe], [O/Fe] and [FeI/H]. The [X/Fe] values change less than 0.25 dex for the change in the ξ by 2.0 km s⁻¹.

Figure 6 shows the abundance ratios ([X/Fe]) as a function of the atomic number.

5.3.1 CNO and Na

The abundance pattern of CRL2688 shows enhancement of C, N, O relative to Fe. The obtained abundance ratios, [C/Fe]= 0.63 ± 0.08 and [O/Fe]= 0.53 ± 0.25 , are in good agreement with those derived by Klochkova et al. (2000).

The carbon abundance is estimated from the five lines with the line-to-line scatter of 0.18 dex. The [C/Fe] does not significantly change by the change in T_{eff} as shown in Table 3.

The oxygen abundance is derived from the O I line at 6158.2 Å. The abundance may be slightly overestimated since this line is blended with a weak Fe I line at 6157.7 Å. By synthesizing a spectrum around this line for this star, the contribution from the Fe I line is estimated to be $\sim 4\%$, which is much smaller than the other errors in [O/Fe]. The derived abundance is also sensitive to the adopted temperature (Table 3). Furthermore, negative non-LTE correction of 0.1 – 0.2 dex is expected for stars with a similar spectral type (Takeda & Takada-Hidai 1998). Therefore, an overabundance of [O/Fe] for this star is not yet clear in the present study.

The [N/Fe] ratio of 1.02 ± 0.25 is significantly lower than that from Klochkova et al. (2000), who derived [N/Fe]= 2.0. Since as indicated in Table 3, the derived [N/Fe] abundance largely depends on the choice of parameters in the model atmosphere, especially in T_{eff} , the difference from Klochkova et al. (2000) may be explained by systematic errors due to the atmospheric parameters as well as by difference in the measured EWs. Moreover, the N abundance

from the N I 7468.3 Å line may suffer from non-LTE effects as suggested by Takeda & Takada-Hidai (1995). The non-LTE analysis by Takeda & Takada-Hidai (1995) suggests that non-LTE corrections for the abundances derived from N I lines around ~ 8700 Å for F-type supergiant stars are ~ -0.4 dex. A similar non-LTE correction is expected for the N I line used in this work. Taking into account a possible non-LTE correction of -0.4 dex, a modest $[N/Fe]$ remains, although the non-LTE calculation is needed for a more reliable estimate.

The Na abundance is estimated from two lines (5682.63 Å and 5688.21 Å). For these lines, Takeda et al. (2003) reported that non-LTE correction to the abundances of their sample stars is less than 0.2 dex, which is not significant within the precision of the present analysis. The derived abundance ratio is $[Na/Fe] = 0.70 \pm 0.14$, which is in agreement with that derived by Klochkova et al. (2000). This value is higher than that observed in most of the previously studied disk stars with similar metallicity, that generally show the solar ratio (Takeda et al. 2003).

5.3.2 Neutron-capture elements

The Y abundance is estimated to be $[Y/Fe] = 1.07 \pm 0.37$ from two lines, where the large error comes from the line-to-line difference in derived abundances. This value is in agreement with that derived by Klochkova et al. (2000) and significantly higher than those observed in typical disk stars with similar metallicity (Edvardsson et al. 1993). Such enhanced $[Y/Fe]$, however, is not unusual for other carbon-rich post-AGB stars (Reyniers et al. 2004; Reddy et al. 1997).

On the other hand, the abundance of the heavier s-process element Ba is not as highly enhanced as that of Y. We note that the Ba abundance was estimated from just one of the three lines detected in our spectrum because the other two lines seem to be affected by the emission in the violet wing (Figure 2). The Ba line at 5853.67 Å has an approximately symmetric profile, which we think it is more reliable. For the group of the heavy s-process elements, we could only obtain the upper limits of the abundances. Enhancements similar to $[Y/Fe]$ are certainly not observed and remain comparable to or lower than the $[Ba/Fe]$ ratio.

The ratio of heavy to light s-process elements is frequently used as a measure of the neutron exposure responsible for processing these elements. The observed $[Ba/Y] = -1.0 \pm 0.4$ is actually very low. This result has also been reported by the previous study of Klochkova et al. (2000). In Figure 7, we compared the abundance pattern of the s-process elements of CRL 2688 in this work with that of other post-AGB stars analyzed by Reyniers et al. (2004). Here we use Ba and Y as a tracer for heavy-s and light-s process elements ($[hs/ls] \sim [Ba/Y]$ and $[s/Fe] \sim ([Y/Fe] + [Ba/Fe])/2$). In Reyniers et al. (2004), the heavy-s process abundance is calculated as the mean of the Ba, La, Nd and Sm abundances, while the light-s process abundance is the mean of the abundances derived from Y and Zr. Figure 7 shows that CRL 2688 has the lowest $[hs/ls]$ compared to the other objects. However, CRL 2688 appears to follow the same linear relation in $[hs/ls] - [s/Fe]$.

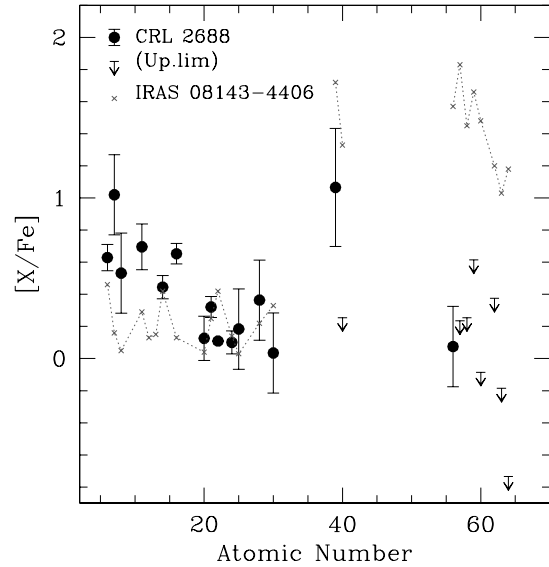


Figure 6. Abundance pattern of CRL2688. Gray crosses and dotted lines show the abundance pattern of another carbon-rich post AGB star IRAS 08143-4406 from Reyniers et al. (2004).

5.3.3 Alpha and Fe-peak elements

The α and Fe-peak elements are normal compared to the values observed in the Galactic disk stars with similar metallicity. In particular, the non-refractory element Zn abundance is estimated to be $[Zn/Fe] = 0.04 \pm 0.25$ dex, which is the standard value observed in disk stars with similar metallicity, suggesting that depletion of refractory elements due to condensation onto dust grains does not significantly contribute to the observed abundance pattern. Another non-refractory element, sulphur, shows an enhanced abundance ratio of $[S/Fe] = 0.65 \pm 0.06$ consistent with the previous analysis made by Klochkova et al. (2000). This value is higher than typical values reported for disk dwarf/giant stars with similar metallicity studied by Takeda & Takada-Hidai (2011), that generally show the solar ratio. Since the sulphur abundance is measured from relatively weak lines, a higher signal-to-noise ratio spectroscopy is needed to confirm the overabundance of $[S/Fe]$.

6 DISCUSSION

6.1 Circumstellar envelope

The radial velocities of the molecular lines provide an estimation of the velocity of the circumstellar outflow where these lines are formed. The emission components of the C₂ Phillips bands have a mean radial velocity of -38.1 km s⁻¹ with respect to the photospheric atomic absorption lines, while the emission components of the H α , Na I (e1) and K I lines have a similar value of -41 km s⁻¹. For the absorption components of the C₂ Phillips bands, this value is -53.0 km s⁻¹, which is in good agreement with the value of -51.8 km s⁻¹ derived from the CN red system. Existence of several velocity components of circumstellar outflows in a range 19-100 km s⁻¹ have been identified based on CO and

Table 3. Abundance results

Elem	[X/H] (dex)	[X/Fe] (dex)	σ_{lines}^a (dex)	N	T_{eff}^b		ξ		
					+400 K	-400 K	+0.5 dex	+2.0 km s ⁻¹	-2.0 km s ⁻¹
C I	0.31	0.63	0.08	5	-0.13	0.20	0.07	-0.01	-0.00
N I	0.70	1.02	—	1	-0.41	0.52	0.24	-0.09	0.16
O I	0.21	0.53	—	1	-0.42	0.56	0.26	-0.06	0.09
Na I	0.37	0.69	0.14	2	-0.08	0.08	0.00	0.00	-0.01
Si II	0.11	0.45	0.07	2	-0.30	0.33	0.05	-0.02	-0.00
S I	0.33	0.65	0.06	3	-0.11	0.13	0.02	0.02	-0.05
Ca I	-0.20	0.12	0.14	4	-0.05	0.05	-0.00	-0.00	0.00
Sc II	-0.01	0.32	0.07	4	0.08	-0.07	0.01	0.00	0.01
Ti II	-0.22	0.11	0.00	2	0.08	-0.07	0.01	0.01	0.00
Cr II	-0.23	0.10	0.07	8	-0.02	0.02	0.01	0.03	-0.08
Mn I	-0.14	0.18	—	1	0.02	-0.01	0.00	0.01	-0.03
Fe I	-0.32	0.00	0.07	13	0.41	-0.44	-0.19	-0.04	0.09
Fe II	-0.34	0.00	0.04	5	0.25	-0.18	0.05	-0.10	0.24
Ni I	0.04	0.36	—	1	-0.02	0.03	0.00	0.00	-0.00
Zn I	-0.29	0.04	—	1	0.00	0.00	0.01	0.03	-0.07
Y II	0.73	1.07	0.37	2	0.08	-0.08	0.00	0.05	-0.10
Ba II	-0.26	0.07	—	1	0.13	-0.11	0.01	-0.07	0.21

^a When only one line is available for the abundance estimate, then an error is taken to be equal to 0.25, which is the line-to-line scatter in abundances derived from individual Fe I lines.

^b Effect of errors in atmospheric parameters on [X/Fe] ratios.

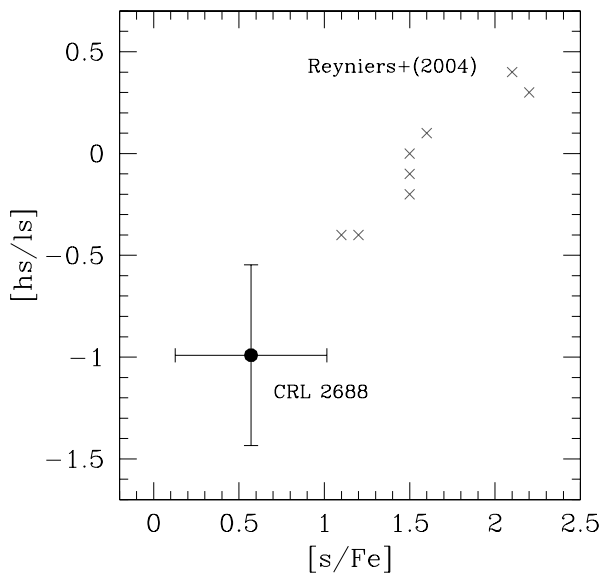


Figure 7. Heavy s-process element to light s-process element ratios plotted against mean of s-process to Fe ratios. In this work (filled circle), [s/Fe] is taken as a mean of [Y/Fe] and [Ba/Fe], while [Ba/Y] ratio is used as a proxy of [hs/ls]. For the data obtained by Reyniers et al. (2004) (gray crosses), the definition from the original paper is used for both quantities.

¹³CO observations at radio wavelengths (Young et al. 1992; Yamamura et al. 1996).

In the circumstellar environment, these molecules are thought to form from more complex molecules like C₂H₂ and HCN that are photodissociated by interstellar and/or stellar radiation fields. Therefore, it is suggested that

these molecules are confined to a thin circumstellar shell whose inner and outer radius are determined by the penetration/shields of photons from the radiation fields (Bakker et al. 1997). The presence of both absorption and emission components in C₂ Phillips bands suggests complex geometric structure of this circumstellar shell in which C₂ and CN can exist. Furthermore, the radial velocity differences between these components indicate that the regions where the absorption components of the C₂ and CN bands arise are expanding faster than those for the emission components.

6.2 Abundance pattern

The enhanced C, N and Na abundances seen in CRL 2688 are indicative of dredge-up and mixing of H and He burning products during the AGB phase of evolution. In this process, freshly synthesized s-process elements are also expected to be dredged-up, giving rise to overabundance in s-process elements in the photosphere. Indeed a class of carbon-enriched post-AGB stars are known to be enhanced with s-process elements (Hrivnak & Reddy 2003; Reyniers et al. 2004). However, not all of them show this enhancement and some stars show depression in the s-process elements instead. The origin of this diversity in s-process abundance patterns is not well understood (e.g. Käppeler et al. 2011). Theoretical models for the generation of s-process elements during the AGB evolution depends strongly on the parametrization of unknown factors such as a ¹³C pocket, which may control neutron exposure (Busso et al. 1999). Busso et al. (1999) also suggested that the s-process efficiency depends on progenitor metallicity.

Reyniers et al. (2004) found a strong correlation of [hs/ls] index with the overall s-process elemental abundance ([s/Fe]) for their sample of carbon-rich post-AGB stars.

They have suggested that the observed variation in the s-process elemental abundance patterns can partly be explained by AGB models with varying strength of the ^{13}C pocket. The observed low $[\text{Ba}/\text{Y}]$, treated as a proxy of $[\text{hs}/\text{ls}]$, appears to follow the suggested $[\text{hs}/\text{ls}]-[\text{s}/\text{Fe}]$ relation but with the lowest estimate of $[\text{hs}/\text{ls}]$, which is lower than typical theoretical predictions (Käppeler et al. 2011). Alternatively, a neutron source of $^{22}\text{Ne}(\alpha, n)^{25}\text{Mg}$, which would operate in rather massive AGB stars, might be responsible for the observed abundance pattern. If this is the case, the progenitor may be a star with more than 3 or 4 solar masses. However this would be in contradiction with the observed C-rich nature of the circumstellar envelope of CRL 2688. Note that the abundance result suggests that $\text{C}/\text{O} < 1$ from the photospheric absorption lines. However, the oxygen lines may be influenced by non-LTE effects. If we apply non-LTE correction to oxygen abundance the C/O ratio may be 1.0 or more.

Since only Y and Ba have reliably been estimated in the present work, the conclusion about the very low $[\text{hs}/\text{ls}]$ remains to be confirmed. Further accurate abundance study with much higher resolution and high signal to ratio spectrum may enable us to understand nucleosynthesis in the progenitor star.

7 CONCLUSION

We have presented the analysis of a high-resolution optical spectrum of CRL 2688. Based on the one-dimensional LTE abundance analysis, we have confirmed that the central star has a spectral type of a F-type supergiant with $[\text{Fe}/\text{H}] = -0.3 \pm 0.1$. Molecular absorptions from C_2 Phillips, C_2 Swan bands and CN red system, that are presumably of circumstellar origin have been identified, some of which appear in emission. In particular, C_2 Phillips band show presence of emission components with the helio-centric radial velocity offsetted from the photospheric absorption lines by -38 km s^{-1} , which is consistent with emission components seen also in the $\text{H}\alpha$ line, Na I and K I resonance lines (-41 km s^{-1}). The absorption components of these lines have a mean radial velocity of -52 km s^{-1} with respect to the photospheric absorption lines, and are more highly blueshifted than the corresponding emission components.

The abundance pattern of CRL2688 is characterized by the enhancement of C, N, Na and Y. However, unlike other known C-rich post AGB stars, this object shows a very low $[\text{Ba}/\text{Y}]$ ratio. Since only abundances of Ba and Y have been reliably measured as a tracer of heavy and light s-process elements, respectively, in the present work, the conclusion about the peculiar $[\text{hs}/\text{ls}]$ ratio observed in CRL 2688 remains to be confirmed with measurements of more heavy and light s-process elements.

Higher resolution and higher signal-to-noise ratio spectroscopy is required for more comprehensive understanding of the origin of the each spectral feature and the detailed abundance pattern.

ACKNOWLEDGMENTS

MP is thankful to Prof. Shoken Miyama for his kind support, encouragement and hospitality. D.A.G.H. and A.M. also acknowledge support provided by the Spanish Ministry of Economy and Competitiveness under grant AYA2011-27754.

This publication is based on observations made on the island of La Palma with the William Herschel Telescope (WHT). The WHT is operated by the Isaac Newton Group (ING) and is located in the Spanish Observatorio of the Roque de Los Muchachos of the Instituto de Astrofísica de Canarias.

REFERENCES

- Aoki, W., Barklem, P. S., Beers, T. C., et al. 2009, *ApJ*, 698, 1803
- Bakker, E. J., Waters, L. B. F. M., Lamers, H. J. G. L. M., Trams, N. R., & van der Wolf, F. L. A. 1996, *A&A*, 310, 893
- Bakker, E. J., van Dishoeck, E. F., Waters, L. B. F. M., & Schoenmaker, T. 1997, 323, 469
- Balick, B., Gomez, T., Vinković, D., Alcolea, J., Corradi, R. L. M., & Frank, A. 2012, *ApJ*, 745, 188
- Busso, M., Gallino, R., & Wasserburg, G. J. 1999, *ARAA*, 37, 239
- Castelli, F., & Kurucz, R. L. 2003, in *IAU Symposium, Modelling of Stellar Atmosphere*, ed. Piskunov, N., 210P, A20
- Cohen, M., & Kuhl, L. V., 1977, *ApJ*, 213, 79
- Cohen, M., & Kuhl, L. V., 1980, *PASP*, 92, 736
- Crampton, D., Cowley, A. P., & Humphreys, R. M., 1975, *ApJ*, 198, 135
- Crawford, I. A., & Barlow, M. J. 2000, *MNRAS*, 311, 370
- Edvardsson, B., Andersen, J., Gustafsson, B., et al. 1993, *A&A*, 275, 101
- Forrest, W. J., Merrill, K. M., Russell, R. W., & Soifer, B. T., 1975, *ApJ*, 199L, 181
- Friedman, S. D., York, D. G., Benjamin, M., et al. 2011, *ApJ*, 727, 33
- Hrivnak, B. J., & Reddy, B. E. 2003, *ApJ*, 590, 1049
- Hrivnak, B. J., Lu, W., Maupin, R. E., & Spitzmart, B. D. 2010, *ApJ*, 709, 1042
- Käppeler, F., Gallino, R., Bisterzo, S., & Aoki, W. 2011, *RvMP*, 83, 157
- Klochova, V. G., Szczerba, R., & Panchuk, V. E. 2000, *AstL*, 26, 439
- Klochova, V. G., Panchuk, V. E., Yushkin, M. V., & Miroschnichenko, A. S. 2004, *ARep*, 48, 288
- Luna, R., Cox, N. L. J., Satorre, M. A., García-Hernández, D. A., Suárez, O., & García-Lario, P. 2008, *A&A*, 480, 133
- Ney, E. P., Merrill, K. M., Becklin, E. E., Neugebauer, G., & Wynn-Williams, C. G. 1975, *APJ*, 198L, 129
- Reddy, B. E., Parthasarathy, M., Gonzalez, G., & Bakker, E. J. 1997, *A&A*, 328, 331
- Reyniers, M., Van Winckel, H., Gallino, R. and Straniero 2004, *A&A*, 417, 269
- Sahai, R., Trauger, J. T., Watson, A. M., et al. 1998, *ApJ*, 493, 301

- Schlegel, D. J., Finkbeiner, D. P., & Davis, M. 1998, ApJ, 500, 525
- Takeda, Y., & Takada-Hidai, M. 1995, PASJ, 47, 169
- Takeda, Y., & Takada-Hidai, M. 1998, PASJ, 50, 629
- Takeda, Y., Zhao, G., Takada-Hidai, M., Chen, Y.-Q. , Saito, Y., & Zhang, H.-W. 2003, CJAA, 4, 316
- Takeda, Y., & Takada-Hidai, M. 2011, PASJ, 63, 537
- Ueta, T., Murakawa, K., & Meixner, M. 2006, ApJ, 641, 1113
- Wesson, R., Cernicharo, J., Barlow, M. M. et al. 2010, A&A, 518, L144
- Yamamura, I., Onaka, T., Kamijo, F., Deguchi, S., & Ukita, N. 1996, ApJ, 465, 926
- Young, K., Serabyn, G., Phillips, T. G., Knapp, G. R., Güsten, R., & Schulz, A. 1992, ApJ, 385, 265